

Catherine L. Stauffer<sup>1\*</sup>, A. A. Wing<sup>1</sup>, and K. A. Reed<sup>2</sup>

<sup>1</sup>Florida State University, Tallahassee, FL; <sup>2</sup>Stonybrook University, Stony Brook, NY

## 1. INTRODUCTION

Radiative-Convective Equilibrium (RCE) is a simplified framework of the tropical atmosphere where radiative cooling is balanced by convective heating. RCE has been used frequently the past couple of decades to study tropical convection, circulation, and climate sensitivity (e.g., Held et al., 1993). The Radiative Convective Equilibrium Model Intercomparison Project (RCEMIP, Wing et al., 2018) utilizes this simple setup allowing for the participation of several types of models including Cloud Resolving Models (CRMs), General Circulation Models (GCMs), Global Cloud Resolving Models (GCRMs), and Large Eddy Simulations (LES). The participating models are all configured in a common framework (Wing et al., 2018) overcoming limitations of previous RCE work that was configured in different ways and therefore that was not directly comparable.

The lack of a common configuration limits the interpretation of past disparate results, such as the uncertainty in whether aggregation of convection changes with warming SST and, if it does, in what way and why (Wing, 2019 and references therein). Self-aggregation of convection is a well documented instability of RCE simulations characterized by clustering of convection without any external influences such as temperature gradients (Wing et al., 2017 and references therein). As overviewed by Wing (2019), aggregated convection dries the mean state and allows for more efficient radiative cooling. This, combined with a possible enhancement of self-aggregation of convection with warming, raises the possibility for a negative climate feedback (Khairoutdinov and Emanuel, 2013; Mauritsen and Stevens, 2015; Hohenegger and Stevens, 2016; Cronin and Wing, 2017).

Motivated by the unprecedented collection of many model types configured in a consistent manner, which allows for a more complete comparison of characteristics of RCE, this work will describe the climate state

of the RCEMIP simulations as well as discuss whether convective self-aggregation changes with warming across the models.

Each model used in this study has simulations at a SST of 295 K, 300 K, and 305 K in both small (un-aggregated convection) and large (aggregated convection) domains, where available. More information on the dataset is provided by Wing et al. (2018, 2020).

## 2. CLIMATE STATE

Using the 300 K simulations as a representative example, Figure 1 shows that aggregated (large domain) simulations have greater precipitation rates (average of  $\sim 3.5 \text{ mm day}^{-1}$  vs.  $\sim 2.75 \text{ mm day}^{-1}$ ), while they have less net radiation entering the top of atmosphere ( $R_{TOA}$ ,  $\sim 70 \text{ W m}^{-2}$  vs.  $\sim 105 \text{ W m}^{-2}$ ), less precipitable water (PW,  $\sim 32 \text{ kg m}^{-2}$  vs.  $\sim 39 \text{ kg m}^{-2}$ ), and a more stable lapse rate ( $\sim 7.0 \text{ K km}^{-1}$  vs.  $\sim 7.5 \text{ K km}^{-1}$ ) than their unaggregated counterparts (as represented by large vs. small simulations, respectively, in Figure 1). The aggregated simulations also have a larger intermodel spread in these variables, except for PW where the spread is greater in the unaggregated simulations.

In general, the RCE state varies widely across the ensemble of models for various climate characteristics including cloudiness and relative humidity, as depicted by the large spread in profiles across the RCEMIP simulations in Figure 2.

## 3. CONVECTIVE SELF-AGGREGATION

We find that, in the large simulations (Figures 3 and 4), convection aggregates to a certain extent in all of the models except WRF-CRM (Figure 3m), which appears to be more regularly distributed. However, the convection exhibits a wide variety of strengths and structures with anything from several convecting “blobs” (e.g. Figure 3e,f or Figure 4g,k), to “banded”/“frontal” features (e.g. Figure 3h,k, Figure 4c), or just one large convecting region surrounded by a large subsiding region (e.g. Figure 3b, Figure 4m).

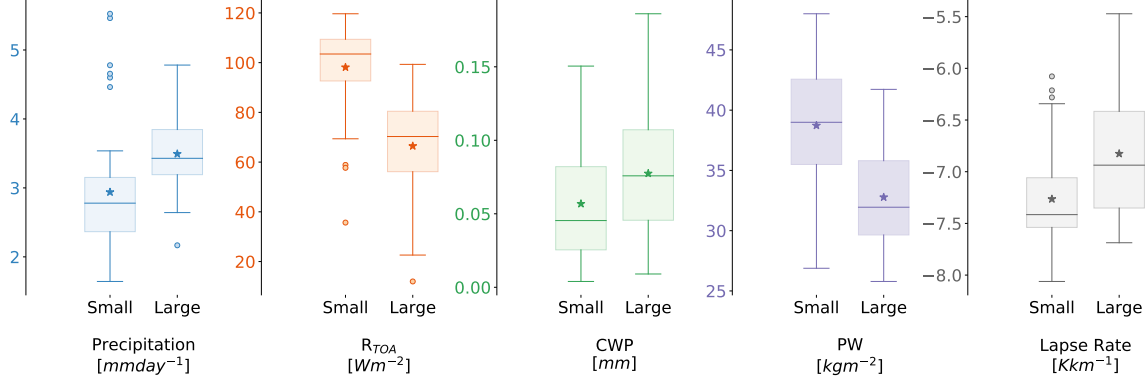
In order to analyze the response of convective aggregation to changing SST we quantify the degree of aggregation that occurs within the simulations using three separate metrics: the organization index ( $I_{org}$ , Tompkins and Semie, 2017), the subsidence fraction ( $f_{sub}$ , Coppin and Bony, 2015), and the spatial variance of column relative humidity ( $\sigma_{CRH}^2$ ).

$I_{org}$  is calculated by identifying deep convective entities as four-point connected convective pixels, following Tompkins

---

\* Corresponding author address: Catherine L. Stauffer, Florida State University, Department of Earth, Ocean and Atmospheric Science, Tallahassee, FL, 32306-4520; e-mail: [cstauffer@fsu.edu](mailto:cstauffer@fsu.edu).

Figure 1: Box and whisker plots of various climate characteristics for both the small domain simulations (left boxes) and large domain simulations (right boxes) where the boxes are the interquartile range, whiskers extend to 1.5 times the interquartile range, circles are outliers beyond the range of the whiskers, the star displays the mean of all the simulations, and the horizontal line within the box depicts the median.



and Semie (2017), where deep convecting pixels are those with an OLR value less than  $173 \text{ Wm}^{-2}$  (Wing et al., 2018). The area under the cumulative distribution function (CDF) of the nearest neighbor distances of the centroids of these convecting entities plotted against the theoretical CDF of a two-dimensional Poisson point process defines the  $I_{org}$  value. For the global simulations,  $I_{org}$  is calculated from only the tropical band,  $30^\circ\text{S}$ - $30^\circ\text{N}$ , to account for the impacts of geometry on the nearest neighbor distance calculation.

$f_{sub}$  is the fraction of the domain covered by large-scale subsidence at 500 hPa temporally-averaged over one day and spatially-averaged over  $\sim 100 \text{ km} \times 100 \text{ km}$  bins.

As shown in Figure 5, the response of the degree of aggregation to warming SST not only varies across models, but varies depending on which metric is used for a particular model, as also found in Cronin and Wing, (2017). Close to half of the models have metrics that have conflicting tendencies across the various metrics with no one metric being the cause of conflicting tendencies. This result occurs whether the simulations have parameterized or explicit convection schemes. For those models whose tendencies agree across the metrics, there are twice as many models that have a positive trend.

Similarly, there is no consistent tendency within a given metric. For any of the three metrics, approximately half of the models show a decrease in aggregation with warming while the other half have an increase.

## 4. CONCLUSIONS

The RCEMIP models allow for the exciting comparison of various styles of models configured in the same manner to explore unresolved questions and inconsistencies from past RCE studies related to convection and climate sensitivity. Using this unique suite of models we found that there is a wide spread in the modeled representation of the RCE state and that there is no consensus in the change in aggregation with warming across the models and within a single model using different metrics of aggregation.

## 5. ACKNOWLEDGEMENTS

AAW and CLS acknowledge support from NSF grant 1830724, KAR acknowledges support from NSF grant 1830729. We thank the German Climate Computing Center (DKRZ) for hosting the RCEMIP data.

## 6. REFERENCES

- Coppin, D., and S. Bony, 2015: Physical mechanisms controlling the initiation of convective self-aggregation in a General Circulation Model. *J. Adv. Model. Earth Sys.*, **7**, 2060-2078.
- Cronin, T. W., and A. A. Wing, 2017: Clouds, circulation, and climate sensitivity in a radiative-convective equilibrium channel model. *J. Adv. Model. Earth Sys.*, **9**, 2833-2905.
- Held, I. M., R. S. Hemler, and V. Ramaswamy, 1993: Radiative-convective equilibrium with explicitly two-dimensional moist convection. *J. Atmos. Sci.*,

50, 3909-3927.

- Hohenegger, C., and Stevens, B., 2016: Coupled radiative convective equilibrium simulations with explicit and parameterized convection. *J. Adv. Model. Earth Sys.*, **8**, 1468-1482.
- Khairoutdinov, M. F., and Emanuel, K., 2013: Rotating radiative-convective equilibrium simulated by a cloud-resolving model. *J. Adv. Model. Earth Sys.*, **5**, 816-825.
- Mauritsen, T., and Stevens, B., 2015: Missing iris effect as a possible cause of muted hydrological change and high climate sensitivity in models. *Nature Geoscience*, **8**, 346-351.
- Tompkins, A. M., and A. G. Semie, 2017: Organization of tropical convection in low vertical wind shears: Role of updraft entrainment. *J. Adv. Model. Earth Sys.*, **9**, 1046-1068.
- Wing, A. A., K. Emanuel, C. E. Holloway, and C. Muller, 2017: Convective self-aggregation in numerical simulations: A review. *Surveys in Geophysics*, **38**, 1173-1197.
- Wing, A. A., K. A. Reed, M. Satoh, B. Stevens, S. Bony, and T. Ohno, 2018: Radiative-Convective Equilibrium Model Intercomparison Project. *Geosci. Model Dev.*, **11**, 793-813.
- Wing, A. A., 2019: Self-aggregation of deep convection and its implications for climate. *Curr. Clim. Change Rep.*, **5**, 1-11.
- Wing, A. A., and Coauthors, 2020: Clouds and convective self-aggregation in a multi-model ensemble of radiative-convective equilibrium simulations. *in preparation*.

Figure 2: Vertical profiles for domain-averaged cloud fraction (left) and relative humidity (right) averaged over the simulation neglecting the first 75 days. Small domain simulations are on top, large domain on the bottom.

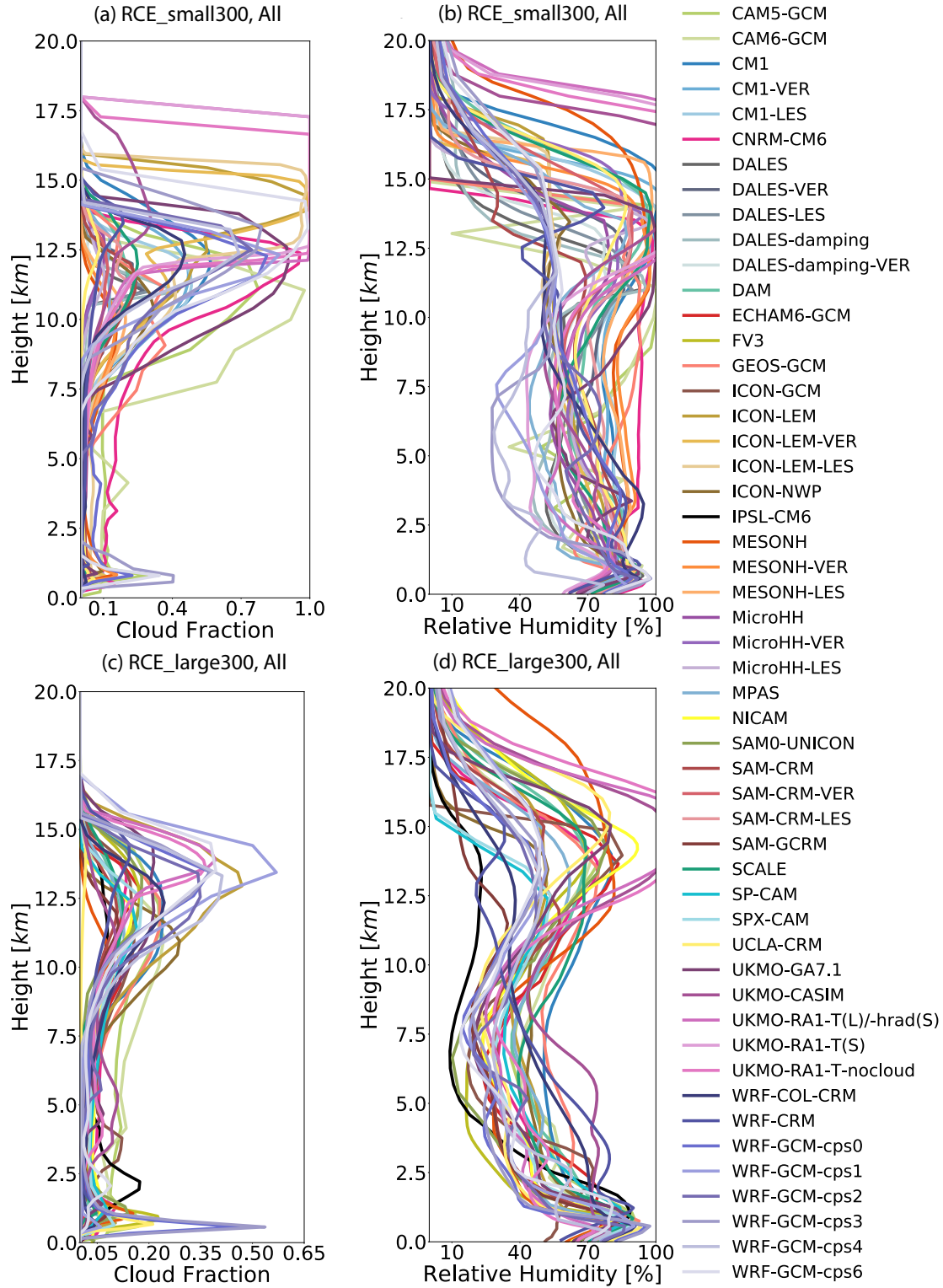


Figure 3: 2-D spatial maps of hourly-averaged outgoing longwave radiation (OLR) on day 80 for large domain CRM simulations. The domains are  $\sim 6000$  km  $\times$   $\sim 400$  km, depending on the capabilities of a model, and 3 km grid spacing.

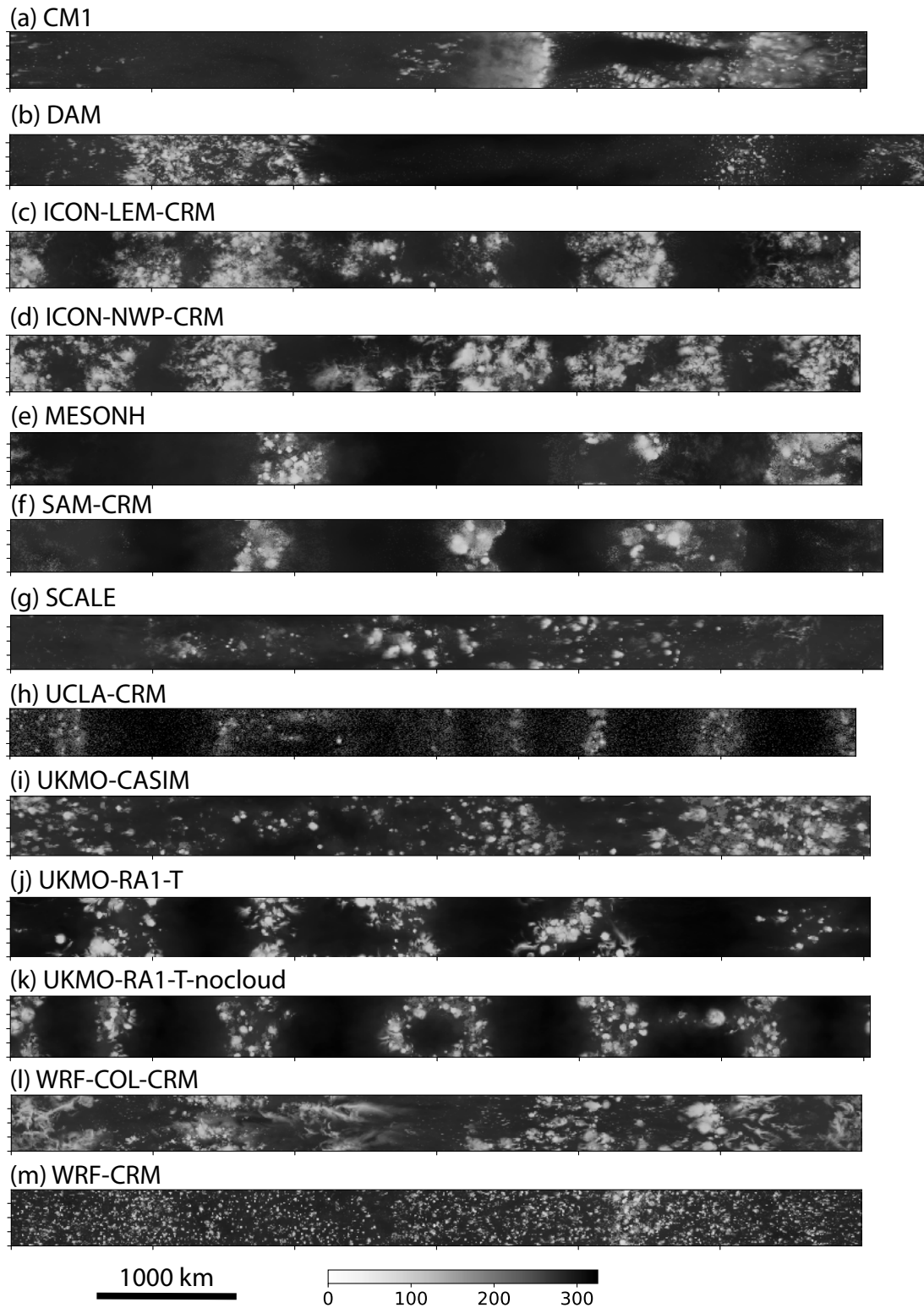


Figure 4: as in Figure 3 except for GCMs (a-k) and GCRMs (l-n). The GCRMs in the box are expanded for easy viewing with their to-scale size outside the box. MPAS (l) has a radius 1/8 that of Earth while NICAM (m) and SAM-GCRM (n) have radii of 1/4 that of Earth.

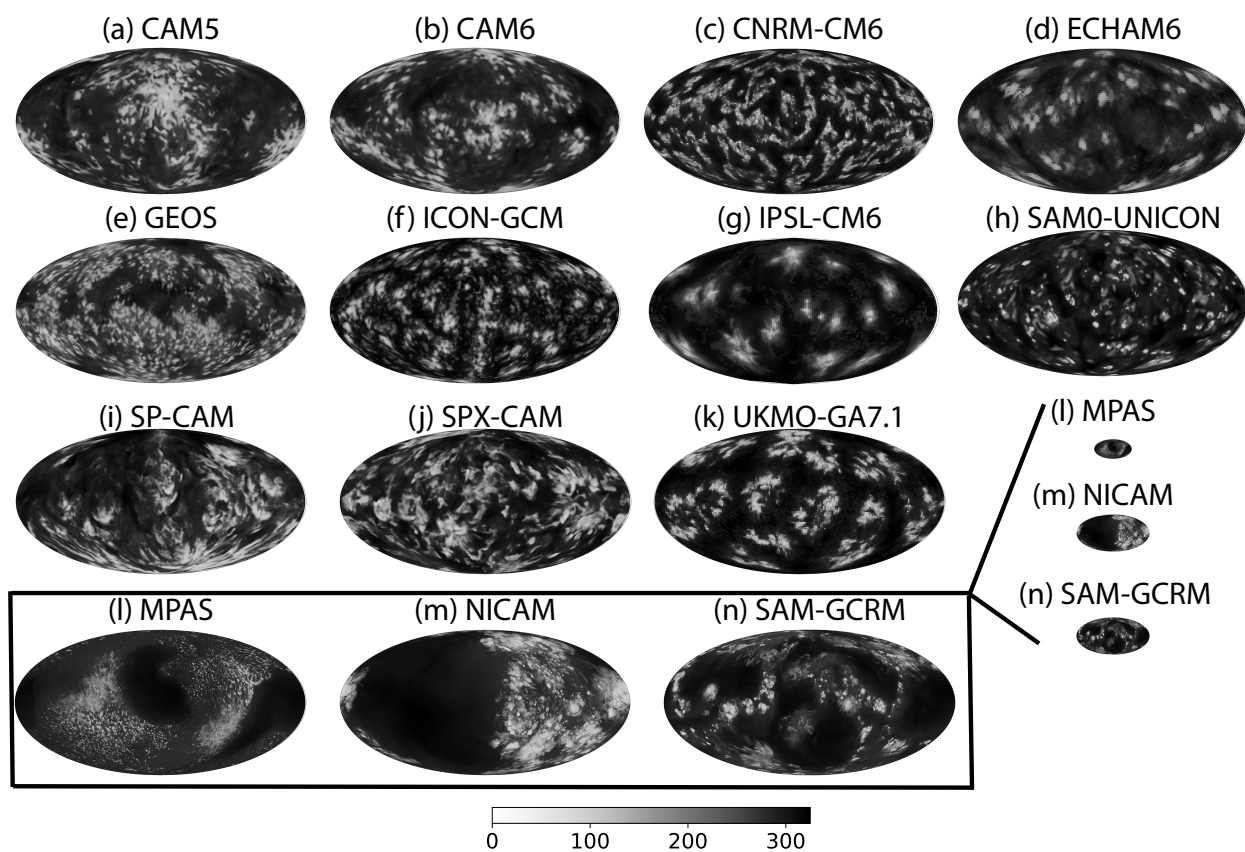


Figure 5: The rate of change of the three metrics of aggregation used in this paper from 295 K-305 K. Red circles are the subsidence fraction, blue squares are the organization index, and the green triangles are the variance in column relative humidity. The box and whisker plots corresponding in color to their respective metrics have a box displaying the interquartile range, whiskers extending to 1.5 times the interquartile range, a horizontal line indicating the median value, and symbols to indicate outliers.

